EARTH SURFACE PROCESSES AND LANDFORMS, VOL. 21, 589–605 (1996)

WIND-TUNNEL MODELLING OF THE INFLUENCE OF VEGETATION STRUCTURE ON SALTATION THRESHOLD

H. BRAD MUSICK[1]*, STEVEN M. TRUJILLO[2] AND C. RANDALL TRUMAN[2]

[1] *Department of Biology, and* [2] *Department of Mechanical Engineering, University of New Mexico, Albuquerque, New Mexico 87131, USA*

Received 28 March 1994
Revised 10 January 1995

ABSTRACT

The influence of vegetation structure on saltation threshold was investigated using uniformly spaced arrays of non-erodible roughness elements on a bed of erodible sand in an wind tunnel. Structural variables tested using arrays of solid cylinders included element aspect ratio (height/diameter) and lateral cover (total frontal-silhouette area per unit ground area). In agreement with previous studies, increase in saltation threshold above the value for bare sand was strongly related to lateral cover. Increasing aspect ratio from 0·25 to 4 tended to enhance the increase in saltation threshold at a given lateral cover. An approximate fit to the results could be obtained using a relation proposed by Raupach *et al.* (*Journal of Geophysical Research*, 1993, **98D,** 3023–3029).

Porous elements were constructed as clusters of narrow, vertically oriented cylinders (model 'stems'), forming porous model plant bodies that were cylindrical in overall shape. Low-porosity elements were found to be approximately 50 per cent more effective in increasing saltation threshold than either solid or high-porosity elements. The ratio of plant-body frontal-silhouette area (based on overall dimensions) to total stem frontal-silhouette area was found to be a useful measure of plant-body porosity for wind erosion studies. Some conventional measures of vegetation amount fail to account for changes in vegetation structural attributes that may strongly influence aeolian processes.

KEY WORDS saltation threshold; vegetation cover; wind erosion; aspect ratio; porosity

INTRODUCTION

One way in which global change may influence aeolian processes is through changes in the degree of protection provided by vegetation against aeolian sediment transport. Arid and semiarid regions contain large areas of sparsely vegetated dune fields and sand sheets where previous sorting by wind has produced a particle size distribution preconditioned for susceptibility to wind transport (McCauley *et al.*, 1981; Otterman and Gornitz, 1983). If the amount of vegetation on these vulnerable surfaces is reduced by drought or changes in land use, aeolian sediment transport could greatly increase (Muhs and Maat, 1993). Conversely increases in vegetation in response to reduced aridity or possibly to increased atmospheric CO_2 concentration (Bazzaz, 1990) could lead to stabilization of currently active dune fields and sand sheets.

Monitoring and predicting the effects of global change on aeolian processes requires models and predictive relations for the influence of vegetation. Models developed specifically for croplands (e.g. Woodruff and Siddoway, 1965) are often difficult to apply to naturally vegetated surfaces. This paper is concerned with the development of predictive relations for application to the natural or spontaneous vegetation cover of arid and semiarid lands.

Wind-tunnel experiments using arrays of model roughness elements to simulate vegetation were

* Current address: 625 Florida St SE, Albuquerque, NM 87108, U.S.A.

CCC 0197-9337/96/070589-17

conducted to determine the quantitative influence of vegetation structural attributes on saltation threshold. To this end, the influence on saltation threshold of lateral cover (also known as roughness density), element aspect ratio AR (= height/diameter), and element porosity were examined.

APPROACH

Vegetation effects on saltation threshold

Marshall (1970, 1971) used shear stress partitioning theory (Schlichting, 1936) to provide a theoretical basis for understanding the aerodynamic influence of vegetation on saltation threshold. This theory partitions wind shear stress on a vegetated surface between stress on the non-erodible roughness elements (i.e. vegetation) and stress on the intervening ground surface. Because a portion of the total shear stress is absorbed by vegetation, the total shear stress on the vegetated surface at the threshold for sediment transport is greater than if the surface was bare. Shear stress τ is related to friction velocity u_* as:

$$\tau = \rho u_*^2 \tag{1}$$

where ρ is air density. For terrestrial surfaces, the small effects of variation in air density are commonly ignored, and thresholds are expressed in terms of u_* (as u_{*t}) rather than τ.

The threshold friction velocity of a surface with non-erodible roughness elements or vegetation (u_{*tR}) is usually greater than the threshold friction velocity that the same erodible surface would have if bare (u_{tS}). Ratioing these thresholds yields a convenient measure of the effect of vegetation. Lyles *et al.* (1974) used the ratio u_{tR}/u_{*tS}, which they termed critical friction velocity ratio (*CFVR*). Others (Musick and Gillette, 1990); Raupach *et al.*, 1993) used the inverse of *CFVR*, denoted as R_t in the latter study. The present study uses the ratio suggested by Lyles *et al.* (1974), but denotes this as R_t^{-1} to avoid use of an acronym while maintaining agreement with previously used notation (Raupach *et al.*, 1993):

$$R_t^{-1} = CFVR = \frac{u_{*tR}}{u_{*tS}} \tag{2}$$

The R_t^{-1} form of the ratio is preferred here because it expresses the multiplicative factor by which the presence of roughness elements raises the threshold. Use of either ratio as a measure of vegetation effects ensures independence from soil properties, such as moisture content or particle size distribution.

Studies of the effect of vegetation on saltation threshold are justified for several reasons. Because moderately strong winds are more frequent than extreme winds, small changes in wind threshold may result in great changes in the frequency and duration of sediment transport. Vegetation also reduces saltation mass flux once the threshold has been exceeded (Ven *et al.*, 1989) by intercepting saltating particles and by reducing shear stress on the erodible surface (Hagen and Armbrust, 1994). Ratios of threshold friction velocities, such as R_t^{-1}, provide a means of estimating the reduction in soil-surface shear stress and are therefore useful in predicting the reduction in mass flux on vegetated surfaces (Hagen and Armbrust, 1994).

Previous studies using solid roughness elements

Shear stress partitioning and the increase in threshold friction velocity are dependent on structural attributes of the vegetation. Wind-tunnel experiments using arrays of model roughness elements to simulate vegetation have been useful in identifying relevant structural variables and quantifying their effect.

Marshall (1971) found that the protective influence of roughness arrays was largely a function of lateral cover λ (also known as roughness density or frontal area index), defined as total frontal silhouette area of roughness elements per unit of ground area over which the array is distributed. Marshall (1971) concluded that roughness-element shape, form and arrangement were of secondary importance.

Field studies indicate that Marshall's results overestimate the protective effect of sparse vegetation (Glendening, 1977; Ash and Wasson, 1983; Eldridge, 1988; Musick and Gillette, 1990). Results of wind-tunnel studies by Lyles *et al.* (1974), Lyles and Allison (1975, 1976), Gillette and Stockton (1989), Ven *et al.* (1989; as analysed in Hagen and Armbrust, 1994), and Iversen *et al.* (1991) confirm the importance of λ

but predict less increase in u_{*t} than Marshall. However, these studies differ regarding the specific quantitative relations between λ and R_t^{-1}. Comparison of the results of these wind-tunnel experiments has been complicated by differing methodologies.

Raupach *et al.* (1993) account for the differences among previous experiments through a relation in which the influence of λ on saltation threshold is modified by three additional variables:

$$CFVR = \sqrt{(1 - m\sigma\lambda)(1 + m\beta\lambda)} \tag{3}$$

Here, σ is the ratio of roughness-element basal to frontal-silhouette areas; β is the ratio of isolated-element (C_r) and bare ground surface (C_s) drag coefficients. The empirical factor m accounts for the increased difference between maximum and mean shear stress on the erodible surface resulting from flow around roughness elements. With an increase in this difference, a lower mean stress is required to initiate saltation. A value of $m = 1$ indicates uniformity of surface shear stress distribution equal to the case for no roughness present; decreasing values for m imply decreasing uniformity.

The role of σ in Equation 3 is to account for effects of the elements covering a portion ($= \sigma\lambda$) of the erodible surface. The fraction of the total drag that is not absorbed by the roughness elements acts only on the portion of the erodible surface that is not covered by the bases of the roughness elements (i.e. on the fractional area $1 - \sigma\lambda$). Confining a given amount of drag to a smaller area increases shear stress and lowers the saltation threshold. When roughness elements are added to a surface, there are two opposing effects on shear stress upon the exposed erodible surface:

(1) the drag force on the soil is reduced as a function of element frontal-silhouette area;
(2) the drag force not absorbed by the roughness elements is confined to an increasingly small area, tending to 'amplify' shear stress on the exposed surface as a function of element basal area (Raupach *et al.*, 1993).

The first of these effects outweighs the second in all but extreme cases. However, the second effect leads to predictions that, for a given λ, elements with a high ratio of basal-to-frontal area (σ) will be less effective in raising the saltation threshold than elements with low σ (Raupach *et al.*, 1993). Increasing the fraction of soil covered by a sparse array of plants will not necessarily increase (and may decrease) the saltation threshold, depending on the concomitant changes in λ.

Equation 3 explicitly specifies that one way in which roughness-element aspect ratio AR (height/diameter) will affect saltation threshold is through differences in σ, which for objects symmetric about the vertical axis is inversely proportional to AR. The present experiments with solid roughness elements were designed, in part, to determine whether element AR has any influence on saltation threshold in addition to the effect accounted for by the σ term as it appears in Equation 3. As applied to Equation 3, the question is whether AR might also influence saltation threshold through differences in element drag coefficient (in β) or in shear stress non-uniformity (in m).

Plant bodies modelled as porous roughness elements

To apply the results of wind-tunnel experiments in which vegetation is physically modelled as an array of roughness elements of simple shape, some correspondingly simple conceptual model of vegetation structure must be adopted. In most arid-land vegetation, leaves and stems are strongly aggregated into individual plant bodies widely separated by bare soil. Arid-land vegetation is therefore appropriately modelled as an array of discrete individual plant bodies. Arrays may be characterized structurally by plant-body population density and arrangement, and plant bodies may be characterized by size, shape, form, porosity and other characteristics (Fuchs, 1979).

Arid-land plant bodies vary widely in porosity, from truly solid to porosities so extreme that mutual aerodynamic sheltering of leaves and stems is unlikely. Previous wind-tunnel studies of roughness-element effects on saltation threshold have not examined the influence of porosity. Aerodynamic studies of porous bodies suggest that porosity could affect saltation threshold through effects on bulk momentum absorption, as indicated by changes in drag coefficient (Hagen and Skidmore, 1971; Landsberg and Thom, 1971; Grant, 1984), and through effects on the temporal and spatial variation in shear stress on the erodible surface (Plate 1971; Laws and Livesey, 1978). The net effect of porosity on saltation threshold cannot be predicted from these

previous studies because they lack one or more features of the physical system in question. These features include three-dimensionality of discrete porous objects, a turbulent boundary layer, and saltation or surface shear stress as a measured variable.

A key problem is to determine the appropriate structural measure of porosity. For two-dimensional bodies such as screens or fences, porosity is readily defined as the unobstructed fraction of frontal-silhouette area. However, the complexity of structure possible in three-dimensional porous bodies permits a number of alternative independent measures of porosity. There is insufficient evidence to show which of these alternative measures is most appropriate in describing the effect of roughness-element porosity on saltation threshold.

A limited series of wind-tunnel experiments was conducted to examine the influence of roughness-element porosity on saltation threshold. The potential magnitude of porosity effects, the form of the relation between porosity and saltation threshold, and the choice of an appropriate structural measure of porosity were investigated.

METHODS

Wind tunnel procedures

The experiments were performed in the 1 m × 1 m × 14·5 m wind tunnel at the U.S. Department of Agriculture Research Station in Big Spring, Texas. This open-circuit suction wind tunnel has a large test section and a long upstream fetch ($\sim$ 10 m) suitable for developing and conditioning a thick turbulent boundary layer required to simulate an atmospheric boundary layer. The tunnel is specifically designed for wind erosion studies, and therefore is equipped to contend with blowing sand particles.

Cylindrical roughness elements (described below) were affixed to a base plate 4·88 m in length. For each test, a homogeneous layer (< 1 mm thick) of oven-dried, sieved sand (particle diameter < 0.84 mm) was sprinkled onto the base plate. The wind was then gradually increased until sand movement was observed. The wind velocity profile was then measured using a rake of pitot-static tubes connected to differential pressure manometers.

Care was taken to develop a turbulent boundary layer of sufficient thickness that the roughness elements would not extend above the logarithmic region. To this end, the wind-tunnel boundary layer was tripped to a turbulent state immediately downstream of the inlet contraction by an array 2·8 m in length of hemispherical roughness elements 22·5 mm in radius; λ of this array was 0·031. Further conditioning of the boundary layer was accomplished by placing an array 5·5 m in length of the same hemispherical elements directly upwind of the test array. λ of this conditioning array was 0·008. This treatment was intended to reduce the distance required for the boundary-layer wind profile to adjust to the roughness array in the test section. The geometry of the tripping and conditioning arrays of roughness elements was constant for all tests. The boundary layer thickness over the roughness field was found to be generally about 30 cm over elements of 12·7 mm or greater height.

Seven pitot-static probes were positioned across the boundary layer from below the roughness element height (typically 6 mm) up to just outside the inner layer of the boundary layer (typically 150 mm). The probes were positioned with approximately equal spacing in log (height).

Only those measurements from probes determined to lie within the logarithmic region of the boundary layer were used to determine u_{*t}. Five probes were normally used, with no fewer than four probes used in any case. For the taller roughness elements, the lowest probe used in the fit was typically just below the plane of the roughness element tops. The probe array was located at the downstream edge of the roughness field midway between two roughness elements and thus immediately downstream of an element in the upstream row. By positioning the rake in different locations, it was found that the probes were far enough downstream that the wake of the upstream element had no noticeable effect on the profile measurement. Upper probes were excluded from the fit when they were estimated to deviate significantly from the logarithmic law, as determined by Cole's wake profile (White, 1991). Thus the logarithmic fit was applied to velocities determined from four to six differential pressure measurements made from near the top of the roughness elements (6 to 50 mm) up to about 100 mm. Replicate u_{*t} measurements were eliminated if the logarithmic curve fit gave a value of $r^2 < 0.95$.

The primary means of determining the onset of sand movement was visual observation. Two other methods were used to provide supporting evidence of sand movement. Following a procedure used by Fryrear (pers. comm.), strips of double-sided sticky tape were placed flat on the bed surface near the downwind end of the test section and capture of saltating grains by the tape was visually observed. A Sensit^{TM} eroding mass flux monitor was also placed at the downwind end of the test section. This device uses a ring-shaped piezoelectric sensor mounted on a post to detect the impact of saltating particles (Stockton and Gillette, 1990). The criterion for threshold was observation of continuous movement of sand occurring uniformly across the width of the tunnel test section.

Although definition of saltation threshold is somewhat arbitrary (Nickling, 1988), R_t^{-1} is a ratio of thresholds and should be relatively insensitive to the criterion for the onset of particle movement if the selected criterion is applied uniformly (Raupach *et al.*, 1993). To minimize errors arising from inconsistency in determining the onset of saltation, the mean u_{*tR} for each configuration of roughness elements was determined from a minimum of five replicate determinations. The mean value of u_{*tS} was observed to be $23{\cdot}7\,\mathrm{cm\,s^{-1}}$.

Roughness element arrays

Cylindrical wooden dowels were used as solid roughness elements (Figure 1A). Elements were arranged on the base plate in rows normal to the mean flow direction. Alternate rows were offset by half the within-row distance between elements to produce a staggered arrangement.

For these cylindrical elements, the aspect ratio AR is defined as the ratio of cylinder height h to diameter d:

$$AR = \frac{h}{d} \tag{4}$$

For a cylinder, AR is related to the ratio of basal to frontal-silhouette areas σ (see Equation 3) as:

$$\sigma = \frac{\pi}{4}\frac{1}{AR} \tag{5}$$

For uniform cylindrical elements, lateral cover λ simplifies to:

$$\lambda = \frac{hdN}{\Lambda} \tag{6}$$

where N cylinders, each of height h and diameter d are arrayed over an area Λ.

Dimensions of the solid roughness element arrays tested are given in Table I. λ values ranged from 0·00098 to 0·25, and AR ranged from 0·25 to 4·0. Two or three different values of AR were tested at most levels of λ. Element diameters ranged from 3·175 mm to 50·8 mm.

For small-scale experimental models to adequately simulate wind-induced saltation phenomena, a number of dimensionless variables should not differ significantly from full-scale values (Kind, 1976; Iversen, 1980). Constraints of wind-tunnel experimentation rarely allow these similitude requirements to be met simultaneously, and some compromise must be adopted. The selection of roughness array dimensions was designed to permit a limited experimental test of the adequacy of scaling. Nine pairs of arrays were geometrically identical except for a twofold difference in absolute size and spacing. Thus, each paired array had the same λ and element AR, but pair members were scale models of each other (Table I). Although the scale difference between members of an array pair was small relative to that between the experimental models and natural vegetation, finding a consistent and significant difference in R_t^{-1} between arrays of differing scale would indicate methodological problems severely limiting application of the results to field phenomena.

Porous roughness elements were constructed as clusters (model plant bodies) of uniform, small-diameter, vertically oriented cylinders (Figure 1B–D). The narrow cylinders constituting each cluster are henceforth termed model 'stems', although they serve as models of any rigid plant-body structural components. Model stems were spaced equidistant from one another within a circular area on the base plate so that overall form of the porous elements was cylindrical. Elements were arranged in staggered rows, and the pattern of stem placement within elements was varied throughout the array. To facilitate comparison with solid-element

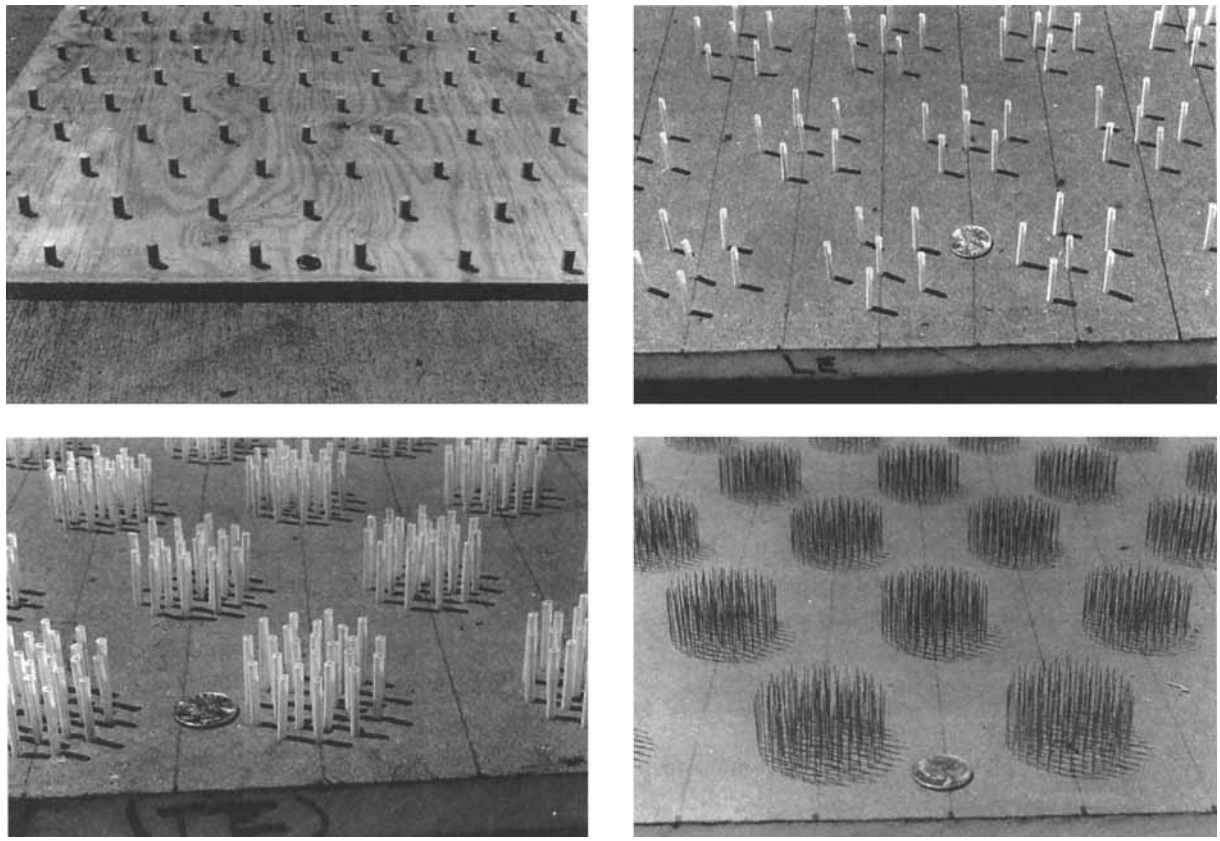

Figure 1. (A) Example of solid-element array: $AR = 2$, $d = 12.7$ mm, $\lambda = 0{\cdot}03125$; (B) porous-element array 2; (C) porous-element array 4; (D) porous-element array 5. For all porous elements, $d = 50{\cdot}8$ mm and $h = 25{\cdot}4$ mm; other dimensions given in Table II

arrays, porous-element arrays were constructed so that overall element dimensions and λ (calculated on the basis of overall dimensions; Table II) were identical to those of two solid-element arrays previously tested ($AR = 0{\cdot}5$, $\lambda = 0{\cdot}03125$ and $0{\cdot}125$; Table I).

The general design of the porous elements (clusters of vertically oriented narrow cylinders) was not intended to provide a highly realistic simulation of any specific natural plant structure. This design was chosen because it entailed a minimal increase in structural complexity over solid elements, and thereby introduced a minimum of new structural variables to be examined.

Because of the labour required to assemble large numbers of porous elements, only a limited number of arrays was tested. In arrays 1–4 (Table II), model stem height h_s (= h) and diameter d_s were held constant, porosity was varied by changing the number of stems per element n_s, and λ was varied by changing the number of porous elements per unit floor area. Two levels of porosity were tested and compared with solid elements at two levels of λ.

The dimensionless measure of element porosity used here is P_f, the ratio of the overall frontal-silhouette area of each element hd to the total stem frontal-silhouette area F_s. For the structure of our porous elements:

$$F_s = h_s d_s n_s \tag{7}$$

and

$$P_f = \frac{hd}{F_s} = \frac{hd}{h_s d_s n_s} \tag{8}$$

Table I. Structural parameters of arrays of solid cylindrical roughness elements. Arrays denoted by the same letter differed twofold in scale but were otherwise structually identical. AR = element aspect ratio, d = element diameter.

Scale pair	AR	d (mm)	λ
	0·25	25·4	0·00391
	0·25	50·8	0·01563
	0·5	12·7	0·00195
A	0·5	12·7	0·00781
A	0·5	25·4	0·00781
	0·5	50·8	0·03125
	0·5	50·8	0·125
	1	6·35	0·00098
B	1	6·35	0·00391
B	1	12.7	0·00391
C	1	12·7	0·01563
C	1	25·4	0·01563
D	1	25·4	0·0625
D	1	50·8	0·0625
	1	50·8	0·25
E	2	3·175	0·00195
E	2	6·35	0·00195
F	2	6·35	0·00781
F	2	12·7	0·00781
G	2	12.7	0.03125
G	2	25·4	0·03125
	2	25·4	0·125
H	4	3·175	0·00391
H	4	6·35	0·00391
I	4	6·35	0·01563
I	4	12·7	0·01563
	4	12·7	0·0625

By definition, a non-porous element is considered to be a cluster of an infinite number of stems, and $P_f \rightarrow 0$. P_f for our porous elements was 0·833 (low porosity) and 3·333 (high porosity). P_f is the inverse of a measure of stem and leaf density proposed by Landsberg and Thom (1971) and used in a number of studies (Landsberg and Powell, 1973; Grant, 1984, 1985; Schuepp, 1989). Alternative measures of porosity are discussed following presentation of the results.

The necessity for two parameters (λ and P_f) to characterize porous-element arrays may be questioned.

Table II. Structural parameters of arrays of porous cylindrical roughness elements. For all arrays, $AR = 0{\cdot}5$, $h_s = h = 25{\cdot}4$ mm, $d = 50{\cdot}8$ mm; P_f is an index of element porosity defined in Equation 8

Array	d_s/d	n_s	λ	P_f
1	0·05	6	0·03125	3·333
2	0·05	6	0·125	3·333
3	0·05	24	0·03125	0·833
4	0·05	24	0·125	0·833
5	0·01	120	0·125	0·833

These arrays may alternatively be viewed as arrays of stems, in which case an appropriate measure of roughness is stem lateral cover λ_s where:

$$\lambda_s = \frac{F_s N}{\Lambda} = \frac{h_s d_s n_s N}{\Lambda} \tag{9}$$

Arrays 2 and 3 differed in both porosity and λ, but their fourfold differences in n_s and N/Λ compensated to yield identical values of λ_s. Finding a significant difference in R_t^{-1} between these arrays would validate the need for a two-parameter description of these arrays: either the addition of an aggregation or sheltering parameter to λ_s, or description in terms of λ and porosity.

Array 5 was similar to array 4, except that d_s was reduced fivefold and n_s was increased fivefold (Figure 1D). Arrays 4 and 5 thus had identical levels of stem frontal-silhouette area per element F_s (see Equation 7). Comparison of these two arrays was intended to determine if the combined effects of variation in frontal-silhouette area per stem $h_s d_s$ and in the number of stems per element n_s could be reduced to a dependence on their mathematical product F_s, which is just the denominator of P_f.

RESULTS AND DISCUSSION

Array scale

A twofold difference in array scale had no consistent effect on u_{*tR} (Figure 2). Five of the nine array pairs showed no statistically significant difference in threshold. The four pairs with significant differences (denoted by an asterisk) were evenly divided between those with a higher threshold for the larger-scale arrays and those with a higher threshold for the smaller-scale array.

The statistically significant, but mostly small, differences between members of some pairs probably resulted from lack of complete experimental independence of the replicate measurements. Replicate measurements for a given array were obtained consecutively after the wind tunnel and associated instrumentation were set up. The most likely explanation for the inconsistent pairwise differences is that slight differences in the experimental set-up gave rise to small biases in the replicate measurements for a given array.

For subsequent analyses of AR and λ effects, the replicate measurements for both members of each scale pair were combined. To ensure equal weighting, values from the data set with the larger sample size were randomly deleted where necessary.

Element aspect ratio (AR)

Differences in R_t^{-1} between arrays of different AR were evaluated independently at each of seven levels of λ

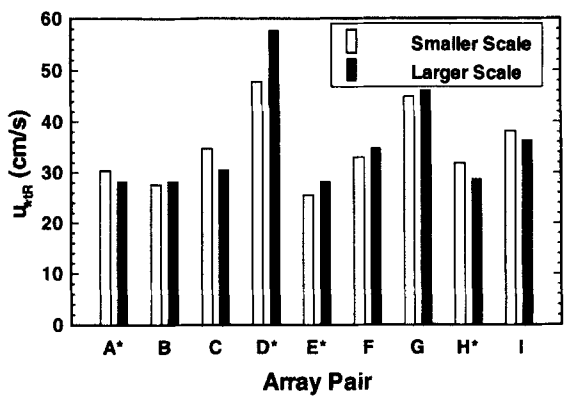

Figure 2. Mean threshold friction velocity (u_{*tR}) for pairs of roughness-element arrays differing twofold in scale but otherwise structurally identical (array parameters given in Table 1). Asterisk indicates statistically significant difference between pair members ($P < 0{\cdot}05$, Mann–Whitney test)

Table III. R_t^{-1} values for arrays of solid roughness elements differing in element aspect ratio AR at a given level of lateral cover λ. Within each column, values denoted by symbol ‡ were not significantly different ($P < 0{\cdot}05$, two-tailed Mann–Whitney test)

	λ						
AR	0·00195	0·00391	0·00781	0·01563	0·03125	0·0625	0·125
0·25		1·12‡		1·36‡			
0·5	1·16‡		1·23		1·87‡		3·18
1		1·19‡		1·38‡		2·22	
2	1·13‡		1·43		1·92‡		3·57
4		1·29		1·59		3·27	

(Table III). In seven of the eleven possible pairwise comparisons, the difference in R_t^{-1} was statistically significant and R_t^{-1} was greater for the higher AR. The influence of AR on R_t^{-1} generally tended to increase with λ.

To determine if the effects of AR on R_t^{-1} shown in Table III could be accounted for solely by differences in amplification of shear stress through variation in exposed area (as accounted for by σ in Equation 3), the measured R_t^{-1} values were normalized for differences in exposed floor area. $(R_t')^{-1}$ is here defined as the value of R_t^{-1} expected if the shear stress going to the floor had been distributed over the entire floor area. An expression for $(R_t')^{-1}$ may be derived from relations given by Marshall (1971) and Raupach *et al.* (1993):

$$(R_t')^{-1} = \frac{R_t^{-1}}{\sqrt{1-\sigma\lambda}} \tag{10}$$

Normalizing for differences in exposed floor area had little effect on R_t^{-1} except at the highest level of λ, and the significant effects of AR were removed by normalization in only one case (Table IV). This finding suggests that reduction in exposed floor area, as accounted for by the σ term in Equation 3, does not fully account for the effects of element aspect ratio (AR) on R_t^{-1}.

Comparison with Raupach et al. (1993)

Results were compared with predictions of Equation 3, the relation proposed by Raupach *et al.* (1993). Predicted R_t^{-1} values were initially calculated using values for β and m recommended by Raupach *et al.* (1993). The value $\beta = 90$ was derived as the ratio $C_r/C_s = 0{\cdot}3/0{\cdot}0033$; the value $C_r \approx 0{\cdot}3 \pm 25$ per cent was presented as an approximate value for cubic, cylindrical and hemispherical roughness elements. The value $m = 0{\cdot}5$ was suggested as the appropriate value for flat topography of the substrate, as in our experiments. Values of σ were determined by AR, as given for cylinders by Equation 5. When calculated using these recommended parameter values, predicted R_t^{-1} values were smaller than observed, as was the predicted effect of AR (Figure 3).

Table IV. Values from Table III converted to $(R_t')^{-1}$ by normalizing for differences in exposed floor area (Equation 10). AR = element aspect ratio, λ = lateral cover. Within each column, values denoted by symbol ‡ were not significantly different ($P < 0{\cdot}05$, two-tailed Mann–Whitney test)

	λ						
AR	0·00195	0·00391	0·00781	0·01563	0·03125	0·0625	0·125
0·25		1·12‡		1·39‡			
0·5	1·16‡		1·24		1·92‡		3·55
1		1·19‡		1·39‡		2·28	
2	1·14‡		1·43		1·93‡		3·66
4		1·29		1·59		3·29	

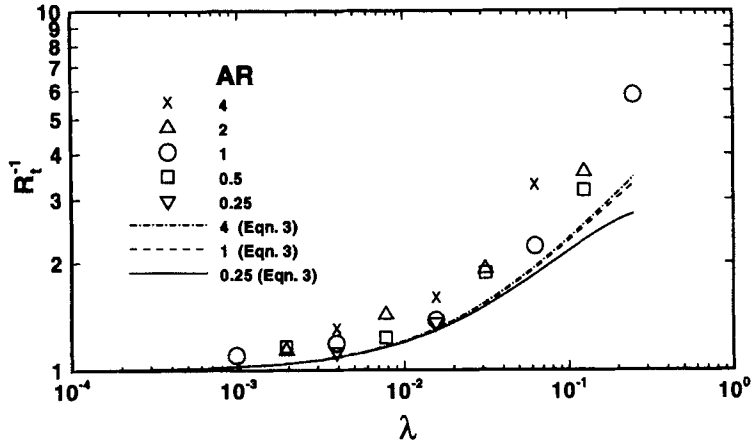

Figure 3. Mean R_t^{-1} for arrays of solid roughness elements; replicates for pairs of arrays differing only in scale were combined after equalizing number of replicates. Curves are predictions from Equation 3 (Raupach *et al.*, 1993) with $\beta = 90$ and $m = 0{\cdot}5$; σ varying with aspect ratio AR according to geometrical relations (Equation 5)

The question then asked was whether agreement of predictions obtained from Equation 3 with the experimental results could be obtained if β and m were assumed to vary with AR. Variation in β was first introduced. Preliminary analyses indicated that variation of ±25 per cent in β (the limits recommended by Raupach *et al.* 1993) was insufficient to obtain agreement of the predictions with the data. Although the evidence is inconsistent, there are some experimental results supporting a nearly twofold increase in C_r as AR increases from 0·33 to 2 (Table V in Marshall, 1971). Twofold variation in β was therefore taken as the maximum possible effect of variation in AR. In Figure 4, C_r and β are increased twofold with an increase in AR from 0·25 to 4, σ again varies with AR according to geometrical relations, while m is held constant at 0·5. Compared to Figure 3, predicted R_t^{-1} values differ more with AR and more nearly agree with the experimental data, but R_t^{-1} is underpredicted in most cases.

Variation in m was then introduced in addition to variation in β. An increase in m implies a decrease in the difference between maximum and mean shear stress on the erodible surface. Previous studies suggest that AR could influence m through changes in the structure of vortices formed in flow around the roughness elements. Patterns of drift topography provide visual evidence of the localized increases in surface shear stress that result when these vortices impinge on the surface. Iversen *et al.* (1991) found that scouring of erodible sedi-

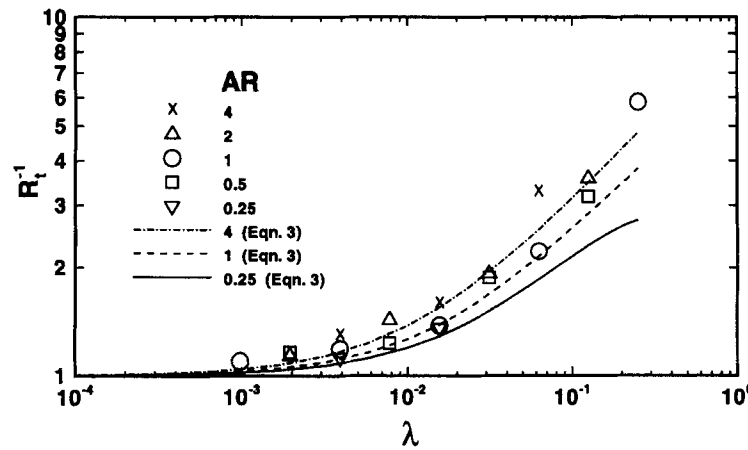

Figure 4. Mean R_t^{-1} for arrays of solid roughness elements; replicates for pairs of arrays differing only in scale were combined after equalizing number of replicates. Curves are predictions from Equation 3 (Raupach *et al.*, 1993) with $m = 0{\cdot}5$; σ varying with aspect ratio AR according to geometrical relations (Equation 5), and $\beta = 90$, 120 and 180 for $AR = 0{\cdot}25$, 1 and 4, respectively

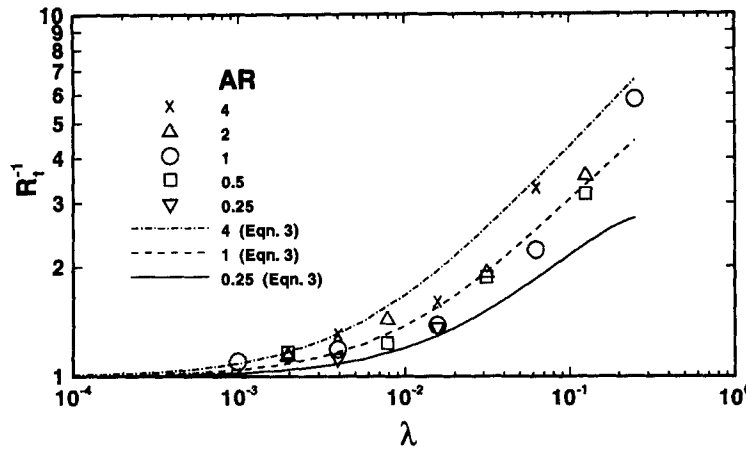

Figure 5. Mean R_t^{-1} for arrays of solid roughness elements; replicates for pairs of arrays differing only in scale were combined after equalizing number of replicates. Curves are predictions from Equation 3 (Raupach *et al.*, 1993), σ varying with aspect ratio AR according to geometrical relations (Equation 5), and $(\beta, m) = (90, 0{\cdot}5)$, (120, 0·5) and (180, 1) for $AR = 0{\cdot}25$, 1 and 4, respectively

ment by trailing vortices shed from the top of the element decreases with increasing element AR, but scouring on the upwind side increases. The net effect of AR on the difference between maximum and mean surface shear stress (and thus m) is therefore difficult to predict.

Because neither the direction nor magnitude of AR influence on m could be predicted from previous studies, it was asked what variation in m would be necessary to account for the experimental results. When m was assumed to increase from 0·5 to 1 as AR increased from 0·25 to 4, the curves of predicted R_t^{-1} diverged more from one another with AR and provided a closer overall fit to the data (Figure 5). This suggests the possibility that element AR influenced R_t^{-1} through variation in m as well as in β and σ. Another possibility is that the form of the predictive equation might require modification, as evidenced by the need to assume extreme and perhaps unrealistic variations in β and m in order to fit Equation 3 to the experimental data.

Element porosity

Experimental results for porous-element arrays and solid-element arrays with the same AR and λ are shown in Figure 6. Except for the comparison of array 4 versus 5, all pairwise differences in R_t^{-1} in Figure 6 were statistically significant ($P < 0{\cdot}05$, Mann–Whitney test).

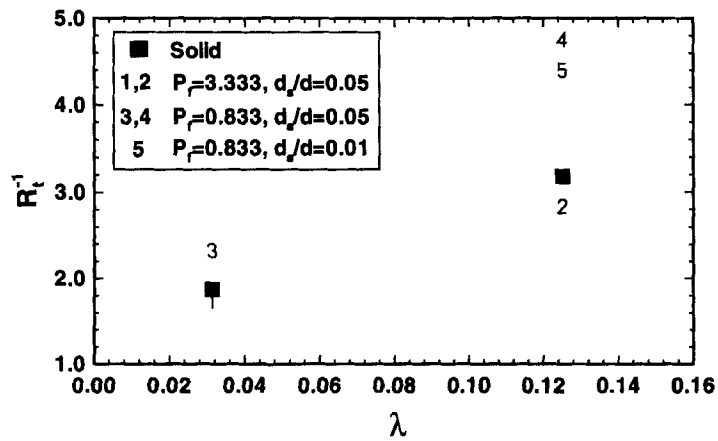

Figure 6. Mean R_t^{-1} for arrays of porous roughness elements (denoted by number in Table II) and of solid elements having the same AR (0·5) and λ. P_f is a measure of porosity (Equation 8). All pairwise differences except 4 *vs.* 5 were statistically significant ($P < 0{\cdot}05$, Mann–Whitney test)

The significant difference between arrays with the same stem lateral cover λ_s (arrays 2 and 3) indicates that λ_s does not adequately account for effects on saltation threshold. Either λ_s must be augmented by an additional parameter expressing the degree of spatial aggregation, or the array must be described in terms of porous-element size and number (by λ) and an additional parameter describing porosity. In subsequent analyses, the latter approach was followed using P_f as the measure of porosity.

Arrays 1–4 (d_s constant) and the comparable solid-element arrays were first examined. At $P_f = 0{\cdot}833$ (arrays 3 and 4), R_t^{-1} was substantially increased over that for solid elements; at $P_f = 3{\cdot}333$ (arrays 1 and 2), R_t^{-1} was decreased below that for solid elements. These results show that maximum R_t^{-1} is obtained at some optimal level of porosity intermediate between nil (solid) and high porosity.

Because the value $R_t^{-1} = 1$ indicates no effect on saltation threshold of a roughness element array, an appropriate measure of the relative effectiveness of two arrays is the ratio of their respective values for the quantity $\{R_t^{-1} - 1\}$. Expressed in this way, the effectiveness of low-porosity elements ($P_f = 0{\cdot}833$) relative to solid elements in raising the saltation threshold was 1·50 at $\lambda = 0{\cdot}03125$ and 1·71 at $\lambda = 0{\cdot}125$. The effectiveness of high-porosity elements ($P_f = 3{\cdot}333$) relative to solid elements was 0·82 at $\lambda = 0{\cdot}03125$ and 0·84 at $\lambda = 0{\cdot}125$. Thus, the influence of a given level of porosity relative to solid elements was relatively uniform at different levels of λ.

Our finding of optimal sheltering at an intermediate level of porosity is also found for two-dimensional barriers (Plate, 1971), but the mechanisms responsible may differ to some degree. Possible mechanisms accounting for the substantially higher R_t^{-1} for low-porosity elements relative to solid elements include increased uniformity of surface shear stress and greater drag of low-porosity elements. Flow through the porous elements would be expected to inhibit the formation or reduce the intensity of the windward 'horseshoe' type vortex and (or) trailing vortices formed by flow around solid cylindrical roughness elements. When wind speeds exceeded threshold levels, sand removal was not observed downwind of the elements, suggesting that trailing vortices did not form or did not impinge on the surface. However, sand was removed from a crescent-shaped region extending into the porous elements up the upwind side, indicating that spatial variation in surface shear stress was not completely eliminated. In the case of two-dimensional barriers, porosity increases the minimum surface shear stress in the lee of the barrier, but lengthens the zone of reduced surface shear stress (Plate, 1971). A similar effect is likely for three-dimensional porous roughness elements.

Whether drag is greater for low-porosity elements than for solid elements is open to question. Drag of long two-dimensional barriers decreases continuously with porosity (Hagen and Skidmore, 1971). However, some studies of three-dimensional objects in freestream flow suggest that drag is increased by a low level of porosity (Alridge *et al.*, 1978). Others have found no clear relation between drag and porosity (Grant, 1984).

Stem size and number

For natural plants, the ratio of stem diameter to plant-body diameter d_s/d might commonly be expected to fall in the range 0·01–0·001. In our porous-element arrays 1–4, the value of this ratio was unrealistically large at 0·05. The lack of significant difference in R_t^{-1} when d_s/d is varied with F_s and P_f constant (array 4 versus array 5 with $d_s/d = 0{\cdot}01$) supports extrapolation of the results from arrays 1–4 to natural plant bodies having smaller but more numerous stems, assuming porosity is measured by P_f or some other expression incorporating F_s.

Porosity indices

Selection of porosity measures for testing may be guided by a number of criteria, including mathematical simplicity and widespread use in other applications. However, the validity of a porosity index is ultimately determined by whether it uniquely accounts for the influence of porosity on the phenomenon of interest.

Comparison of arrays 4 and 5 provides a partial test of the validity of P_f as a measure of porosity for applications to saltation threshold. These arrays had identical levels of stem frontal-silhouette area per element F_s, but the stems in array 5 were five times smaller and five times as numerous. Failure to detect a significant difference in R_t^{-1} between these two arrays (Figure 6) supports F_s ($= h_s d_s n_s$, the denominator of P_f) as a

parameter to express the combined effects of variation in frontal-silhouette area per stem $h_s d_s$ and number of stems per element n_s.

P_f uses element frontal-silhouette area hd as the reference area (numerator in Equation 8) for stem frontal-silhouette area. Other quantities related to overall element size and having dimensions of length squared could be chosen as the reference area. For example, an alternative measure of porosity P_b may be obtained by substituting overall element basal area for element frontal-silhouette area as the numerator of Equation 8:

$$P_b = \frac{\pi r^2}{h_s d_s n_s} \tag{11}$$

P_b is similar to P_f in providing an inverse measure of the 'density' of stem frontal area. However, the change in reference area from frontal in P_f to basal in P_b leads to important differences in how the indices vary with porous-element structure and in relation to aerodynamic properties and saltation threshold.

For example, consider two cylindrical, porous elements having the same stem size and number of stems per unit basal area, but differing twofold in overall element diameter. As measured by P_f, the larger element would be half as porous; as measured by P_b, the two elements would be equally porous. Finding significant aerodynamic and sheltering differences between elements with equal P_b would justify rejection of P_b as a porosity measure. Although experimental proof is lacking for three-dimensional elements in boundary-layer flow, the twofold-longer streamwise path length of the larger element would likely decrease permeability to streamwise flow. Consequent changes in element drag coefficient C_r and in flow structure would likely change the degree of sheltering of an erodible surface.

Another dimensionless index that has been used (Gross, 1987) is volumetric porosity P_v, the ratio of overall element volume to total stem volume per element:

$$P_v = \frac{\pi r^2 h}{\pi r_s^2 h_s n_s} \tag{12}$$

where r and r_s are the radii of element and stem, respectively. Comparison of array 5 with arrays 2 and 4, which had the same λ, is instructive in evaluating this index. According to this measure, roughness elements in array 5 ($P_v = 83{\cdot}33$) would rank highest in porosity, being far more porous than in array 4 ($P_v = 16{\cdot}67$) and slightly more porous than in array 2 ($P_v = 66{\cdot}67$). Explaining the observed variation in R_t^{-1} (Figure 6) as a function of variation in P_v would be extremely awkward. Arrays 4 and 5 differed widely in P_v, but had almost the same effect on saltation threshold. The slight increase in P_v from array 2 to array 5 corresponds to a great increase in R_t^{-1} and would indicate a second peak in the response function. The simplest interpretation is that P_v, in contrast to P_f, is not formulated properly to account for effects of simultaneous variation in its constituent terms (r/r_s and n_s), and thus is unsuitable as an index of porosity in this application.

Streamwise optical (or 'beam') porosity P_o is frequently used to characterize porosity of screens, fences, shelterbelts and other barriers suitable for modelling as two-dimensional objects (Laws and Livesey, 1978; Plate, 1971; Phillips and Willetts, 1979). Use of this measure to characterize natural plant bodies (e.g. Lee, 1991) is appealing because it provides a rapid, non-destructive means of assessing porosity. Relations between plant-body structure and optical porosity are readily derived from numerous previous studies of light transmission through plant canopies (e.g. Federer, 1971; Perry *et al.*, 1988; Li and Strahler, 1988). Beam transmissivity T through an array of small, numerous, randomly distributed, opaque stems is given by:

$$T = \exp(-cp) \tag{13}$$

where c is the volumetric concentration of stem frontal-silhouette area projected in the direction of the beam, and p is the distance through the array. For a cluster of uniform, vertically oriented stems,

$$c = \frac{h_s d_s n_s}{hA} \tag{14}$$

where A is the plan-view area of the cluster.

For a cluster of rectangular plan-view shape with breadth b,

$$A = bp \tag{15}$$

and the optical porosity is:

$$P_o = T = \exp\left(-\frac{h_s d_s n_s}{hb}\right) \tag{16}$$

Substituting the definition of P_f (Equation 8) yields a simple relation between P_o and P_f:

$$P_o = \exp\left(-P_f^{-1}\right) \tag{17}$$

For an element with circular plan-view shape of radius r, the relation between P_o and P_f is more complicated because p (and thus T) varies with spanwise distance x from the centreline of the element:

$$p = 2\sqrt{r^2 - x^2} \tag{18}$$

Integrating across the breadth of the circular element,

$$P_o = \frac{1}{r}\int_0^r \exp\left[-\frac{4}{\pi}P_f^{-1}\frac{\sqrt{r^2 - x^2}}{r}\right]dx \tag{19}$$

For more complexly structured plant bodies, the relation between P_o and P_f may also depend on the arrangement and angular distribution of the plant-body components (Lang, 1987).

Design of the porous elements used in the present study does not permit a comparative evaluation of P_o and P_f because these measures were not varied independently. Further study is needed to determine whether sheltering effectiveness responds to variation in arrangement and orientation of plant-body components in the same manner as does optical porosity.

The major difficulty in characterizing natural plant bodies by means of either P_f or visual porosity is that overall plant-body frontal-silhouette area in an ambiguous quantity for the complex structure of plant bodies. The outline of a plant-body silhouette may be traced with varying degrees of generalization to yield different values for overall frontal-silhouette area. Objective criteria for determination of overall frontal-silhouette area are needed to ensure consistency in measurement of P_f or visual porosity.

IMPLICATIONS: VEGETATION CHANGE AND AEOLIAN PROCESSES

In these experiments, highly simplified structural models of vegetation were used to examine the effects of a few structural attributes thought to influence saltation threshold. Further study is needed to determine the effects of other structural attributes and the response of other saltation processes, particularly sediment mass flux. Additional field studies (Musick and Gillette, 1990; Helm and Breed, *in press*; Wolfe and Nickling, 1996) are needed to test the relations found in this and previous wind-tunnel studies. Nevertheless, the results of this and earlier studies are helpful in predicting how various changes in vegetation might influence aeolian processes.

The most important finding is that various aspects of vegetation structure may strongly influence the level of aeolian sediment transport. Describing vegetation solely in terms of a generalized and non-structural concept of 'amount' is inadequate to characterize changes in structure that may strongly influence aeolian processes. Even the quantitative, specifically defined measures of vegetation amount that are conventionally used in basic and applied vegetation science fail to characterize aspects of structure potentially important for aeolian processes.

This and previous studies (Marshall, 1971; Lyles *et al.*, 1974; Gillette and Stockton, 1989; Iversen *et al.*, 1991; Raupach *et al.*, 1993; Hagen and Armbrust, 1994) have shown that lateral cover λ strongly influences saltation threshold. The relation between saltation threshold and conventional measures of vegetation amount can be predicted if structural relations between those measures and λ are known. If other aspects

of structure are considered secondary in importance to λ and are ignored, these predictions are only approximate, but nevertheless useful for illustrative purposes.

One widely used conventional measure of vegetation amount is percentage canopy cover, which is the percentage of ground area covered by vertical projection of imaginary polygons surrounding each plant crown (Daubenmire, 1968). Here, this measure is expressed as a fraction and referred to as vertically projected cover (*VPC*) to make explicit the distinction from lateral cover λ. Relations between *VPC* and saltation processes have been investigated in laboratory and field experiments (Logie, 1981; Wasson and Nanninga, 1986; Buckley, 1987).

The relation between λ and *VPC* is a function of plant-body form and shape; for cylinders,

$$\lambda = \frac{4}{\pi} \cdot AR \cdot VPC \tag{20}$$

Equation 20 shows that the amount of λ provided per unit of *VPC* increases with *AR*. Increasing *AR* has two effects that tend to increase R_t^{-1} at a given level of *VPC*. One effect derives from purely geometrical considerations (Equation 20), and the second derives from aerodynamic phenomena, whereby R_t^{-1} at a given level of λ is increased (Figures 3–5). The magnitude of the first effect without augmentation by the second effect was estimated by using a single best-fit curve to describe the mean response of R_t^{-1} to λ, and then replotting the response of R_t^{-1} as a function of *VPC*, using Equation 20 to convert λ to *VPC* for different values of *AR*. The curve for $AR = 1$ in Figure 5 was used as an approximation of the mean response of R_t^{-1} to λ (use of mathematically formal curve-fitting procedures was inappropriate in view of the limited range of *AR* tested at high λ). Using this curve in combination with Equation 20 gives predictions of a substantial increase in R_t^{-1} for an increase in *AR* from 0·25 to 4 (Figure 7). This is a conservative estimate of *AR* effects because the greater sheltering of high-*AR* elements at a given λ (Table III, Figures 3–5) is ignored.

It is possible to find strong correlations between saltation threshold and *VPC* when variation in *AR* is limited, because *VPC* is then a surrogate measure of λ. However, the strong influence of *AR* shown in Figure 7 suggests that predictions of R_t^{-1} derived from studies in which *VPC* was used as the measure of vegetation amount and *AR* variation was limited are likely to be in error if applied to plants having a significantly different *AR*.

The predictions shown in Figure 7 challenge intuitive notions concerning the relative importance for aeolian processes of different kinds of change in vegetation. A common assumption (rarely stated explicitly) is that the influence on aeolian processes of changes in plant-body shape and form are generally secondary in importance to changes in vegetation amount. It is commonly further assumed that vegetation amount is characterized reasonably well by conventional measures such as *VPC*. Figure 7 can be used to compare the respective influences of change in *VPC* and plant-body *AR*. Most observers would likely view a decline

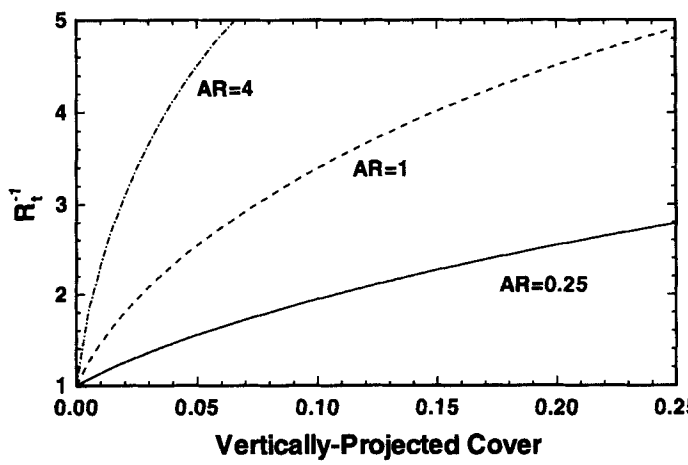

Figure 7. Predicted effect of aspect ratio *AR* on the response of R_t^{-1} to vertically projected cover of cylindrical plants or roughness elements, considering only the influence of *AR* on the amount of λ obtained per unit vertically projected cover (Equation 20)

in *VPC* from 0·2 to 0·05 (with *AR* fixed at 1, for example) as likely to have a far more substantial impact on aeolian processes than a decrease from 1 to 0·25 in plant-body *AR* (with *VPC* constant). However, Figure 7 predicts that these two changes would result in identical reductions in saltation threshold.

Change in plant-body *AR* can result from changes in the species composition of vegetation, if species with one characteristic growth form replace those with another. Even subtle shifts in climate or land use may tip the balance between competing species and lead to major changes in plant species composition. If species replacement results in a change in predominant plant-body shape, the frequency and intensity of sediment transport by wind could be greatly affected. Dependence on the structural attributes of vegetation might thus greatly amplify the response of aeolian processes to global change.

ACKNOWLEDGEMENTS

We thank Dr D. W. Fryrear and staff (U.S. Department of Agriculture, Big Spring, Texas) for use of the wind tunnel and other facilities, for useful suggestions and advice, and for hospitality extended to S.M.T. while working at their laboratory. Funding was provided by the Earth Processes Program of the National Aeronautics and Space Administration (Grant NAG 5–1833) and by a New Mexico Space Grant Fellowship to S.M.T.

REFERENCES

Alridge, T. R. Piper, B. S. and Hunt, J. C. R. 1978. 'The drag coefficient of finite-aspect-ratio perforated circular cylinders', *Journal of Industrial Aerodynamics*, **3,** 251–257.

Ash, J. E. and Wasson, R. J. 1983. 'Vegetation and sand mobility in the Australian desert dunefield', *Zeitschrift für Geomorphologie Suppl. Bd.*, **45,** 7–25.

Bazzaz, F. A. 1990. 'The response of natural ecosystems to the rising global CO_2 levels', *Annual Review of Ecology and Systematics*, **21,** 167–196.

Buckley, R. 1987. 'The effect of sparse vegetation on the transport of dune sand by wind', *Nature*, **325,** 426–428.

Daubenmire, R. 1968. *Plant Communities: A Textbook of Plant Synecology*, Harper and Row, New York, 300 pp.

Eldridge, D. J. 1988. 'Soil-landform and vegetation relations in the chenopod shrublands of western New South Wales', *Earth-Science Reviews*, **25,** 493–499.

Federer, C. 1971, 'Solar radiation absorption by leafless hardwood forests', *Agricultural Meteorology*, **9,** 3–20.

Fuchs, M. 1979. 'Atmospheric transport processes above arid-land vegetation', in Goodall, D. W., Perry, R. A. and Howes, K. M. W. (Eds), *Arid-land Ecosystems: Structure, Functioning, and Management (Volume 1)*, 393–408.

Gillette, D. A. and Stockton, P. H. 1989. 'The effect of nonerodible particles on wind erosion of erodible surfaces', *Journal of Geophysical Research*, **94D,** 12885–12893.

Glendening, J. W. 1977. *Aeolian transport and vegetative capture of particulates*, M.S. Thesis, Colorado State University, Fort Collins, Colorado.

Grant, R. H. 1984. 'The mutual interference of spruce canopy structural elements', *Agricultural and Forest Meteorology*, **32,** 145–156.

Grant. R. H. 1985. 'The influence of the physical attributes of a spruce shoot on momentum transfer', *Agricultural and Forest Meteorology*, **36,** 7–18.

Gross, G. 1987. 'A numerical study of the air flow within and around a single tree', *Boundary-Layer Meteorology*, **40,** 311–327.

Hagen, L. J. and Armbrust, D. V. 1994. 'Plant canopy effects on wind erosion saltation', *Transactions of the ASAE*, **37,** 461–465.

Hagen, L. J. and Skidmore, E. L. 1971. 'Windbreak drag as influenced by porosity', *Transactions of the ASAE*, **14,** 464–465.

Helm, P. J. and Breed, C. S. (in press). 'Instrumented field studies of transport by wind', in Breed, C. S. (Ed.) *USGS Bulletin.*

Iversen, J. D. 1980. 'Drifting-snow similitude—transport-rate and roughness modeling', *Journal of Glaciology*, **26,** 393–403

Iversen, J. D., Wang, W. P., Rasmussen, K. R., Mikkelsen, H. E. and Leach, R. N. 1991. 'Roughness element effect on local and universal saltation transport', *Acta Mechanica Supplementum*, **2,** 65–75.

Kind, R. J. 1976. 'A critical examination of the requirements for model simulation of wind-induced erosion/deposition phenomena such as snow drifting', *Atmospheric Environment*, **10,** 219–227.

Landsberg, J. J. and Powell, D. B. B. 1973. 'Surface exchange characteristic of leaves subject to mutual interference', *Agricultural Meteorology*, **12,** 169–184.

Landsberg, J. J. and Thom, A. S. 1971. 'Aerodynamic properties of a plant of complex structure', *Quarterly Journal of the Royal Meteorological Society*, **97,** 565–570.

Lang, A. R. G. 1987. 'Simplified estimate of leaf area index from transmittance of the sun's beam', *Agricultural and Forest Meteorology*, **41,** 179–186.

Laws, E. M. and Livesey, J. L. 1978. 'Flow through screens', *Annual Review of Fluid Mechanics*, **10,** 247–266.

Lee, J. F. 1991. 'The role of desert shrub size and spacing on wind profile parameters', *Physical Geography*, **12,** 72–89.

Li, X. and Strahler, A. H. 1988. 'Modeling the gap probability of a discontinuous vegetation canopy', *IEEE Transactions on Geoscience and Remote Sensing*, **26,** 161–170.

Logie, M. 1981.'Wind tunnel experiments on dune sands', *Earth Surface Processes and Landforms*, **6,** 365–374.

Lyles, L. and Allison, B. E. 1975. 'Wind erosion: uniformly spacing nonerodible elements eliminates effects of wind direction variability', *Journal of Soil and Water Conservation*, **30**, 225–226.
Lyles, L. and Allison, B. E. 1976. 'Wind erosion: the protective role of simulated standing stubble', *Transactions of the ASAE*, **19**, 61–64.
Lyles, L., Schrandt, R. L. and Schmeidler, N. F. 1974. 'How aerodynamic roughness elements control sand movement', *Transactions of the ASAE*, **17**, 134–139.
Marshall, J. K. 1970. 'Assessing the protective role of shrub-dominated rangeland vegetation against soil erosion by wind', in Norman, M. J. T. (Ed.), *Proceedings 11th International Grassland Congress*, 19–23.
Marshall, J. K. 1971. 'Drag measurements in roughness arrays of varying density and distribution', *Agricultural Meteorology*, **8**, 269–292.
McCauley, J. F., Breed, C. S., Grolier, M. J. and MacKinnon, D. J. 1981. 'The U. S. dust storm of February 1977', in Pewe, T. L. (Ed.), *Desert Dust: Origin, Characteristics, and Effects on Man*, Geological Society of America Special Paper **186**, 123–147.
Muhs, D. R. and Maat, P. B. 1993. 'The potential response of eolian sands to greenhouse warming and precipitation reduction on the Great Plains of the United States', *Journal of Arid Environments*, **25**, 351–361.
Musick, H. B. and Gillette, D. A. 1990. 'Field evaluation of relationships between a vegetation structural parameter and sheltering against wind erosion', *Land Degradation and Rehabilitation*, **2**, 87–94.
Nickling, W. G. 1988. 'The initiation of particle movement by wind', *Sedimentology*, **35**, 499–511.
Otterman, J. and Gornitz, V. 1993. 'Saltation vs. soil stabilization: two processes determining the character of surfaces in arid regions', *Catena*, **10**, 339–362.
Perry, S. G., Fraser A. B., Thomson, D. W. and Norman, J. M. 1988. 'Indirect sensing of plant canopy structure with simple radiation measurements', *Agricultural and Forest Meteorology*, **42**, 255–278.
Phillips, C. J. and Willetts, B. B. 1979. 'Predicting sand deposition at porous fences', *Journal of the Waterway, Port, Coastal and Ocean Division, Proceedings of the Americal Society of Civil Engineers*, **105**, 15–31.
Plate, E. J. 1971. 'The aerodynamics of shelter belts', *Agricultural Meteorology*, **8**, 203–222.
Raupach, M. R., Gillette, D. A. and Leys, J. F. 1993. 'The effect of roughness elements on wind erosion threshold', *Journal of Geophysical Research*, **98D**, 3023–3029.
Schlichting, H. 1936. *Experimentelle untersuchungen zum rauhigkeitsproblem* (English translation), NACA Technical Memorandum **823**.
Schuepp, P. H. 1989. 'Microstructure, density and wetness effects on dry deposition to foliage', *Agricultural and Forest Meteorology*, **47**, 179–198.
Stockton, P. H. and Gillette, D. A. 1990. 'Field measurement of the sheltering effect of vegetation on erodible land surfaces', *Land Degradation and Rehabilitation*, **2**, 77–85.
van de Ven, T. A. M., Fryrear, D. W. and Spaan, W. P. 1989. 'Vegetation characteristics and soil loss by wind', *Journal of Soil and Water Conservation*, **44**, 347–349.
Wasson, R. J. and Nanninga, P. M. 1986. 'Estimating wind transport of sand on vegetated surfaces', *Earth Surface Processes and Landforms*, **11**, 505–514.
White, F. M. 1991. *Viscous Fluid Flow*, 2nd edn, McGraw-Hill, New York, 614 pp.
Wolfe, S. A. and Nickling, W. G. 1996. 'Shear stress partitioning in sparsely vegetated desert canopies', *Earth Surface Processes and Landforms*, **21**, 607–619.
Woodruff, N. P. and Siddoway, F. H. 1965. 'A wind erosion equation', *Soil Science Society of America Proceedings*, **29**, 602–608.